

THE KPNO INTERNATIONAL SPECTROSCOPIC SURVEY.  
IV. H $\alpha$ -SELECTED SURVEY LIST 2.

CARYL GRONWALL<sup>1,2</sup>, JOHN J. SALZER<sup>1</sup>, VICKI L. SARAJEDINI<sup>3</sup>, ANNA JANGREN, AND LAURA  
CHOMIUK<sup>4</sup>

Astronomy Department, Wesleyan University, Middletown, CT 06459; slaz@astro.wesleyan.edu,  
anna@astro.wesleyan.edu

J. WARD MOODY

Department of Physics & Astronomy, Brigham Young University, Provo, UT 84602; jmoody@astro.byu.edu

LISA M. FRATTARE<sup>1</sup>

Space Telescope Science Institute, Baltimore, MD 21218; frattare@stsci.edu

TODD A. BOROSON

National Optical Astronomy Obs., P.O. Box 26732, Tucson, AZ 85726; tyb@noao.edu  
*Submitted 17 November 2003; Accepted 2 January 2004 – To appear in the April, 2004 AJ*

ABSTRACT

The KPNO International Spectroscopic Survey (KISS) is an objective-prism survey for extragalactic emission-line objects. It combines many of the features of previous slitless spectroscopic surveys with the advantages of modern CCD detectors, and is the first purely digital objective-prism survey for emission-line galaxies. Here we present the second list of emission-line galaxy candidates selected from our red spectral data, which cover the wavelength range 6400 to 7200 Å. In most cases, the detected emission line is H $\alpha$ . The current survey list covers a 1.6-degree-wide strip located at  $\delta(1950) = 43^\circ 30'$  and spans the RA range  $11^h 55^m$  to  $16^h 15^m$ . The survey strip runs through the center of the Boötes Void, and has enough depth to adequately sample the far side of the void. An area of  $65.8 \text{ deg}^2$  is covered. A total of 1029 candidate emission-line objects have been selected for inclusion in the survey list ( $15.6 \text{ per deg}^2$ ). We tabulate accurate coordinates and photometry for each source, as well as estimates of the redshift and emission-line flux and equivalent width based on measurements of the digital objective-prism spectra. The properties of the KISS emission-line galaxies are examined using the available observational data. Although the current survey covers only a modest fraction of the total volume of the Boötes Void, we catalog at least twelve objects that appear to be located within the void. Only one of these objects has been recognized previously as a void galaxy.

*Subject headings:* galaxies: emission lines — galaxies: Seyfert — galaxies: starburst — surveys

1. INTRODUCTION

Objective-prism surveys for extragalactic emission-line and/or UV-excess objects have been a fruitful and efficient method for cataloging galaxies with high levels of activity (both star formation and active nuclei) for many years. Most surveys of this kind have utilized photographic plates as their detectors (e.g., Markarian 1967; Smith, Aguirre, & Zelman 1976; MacAlpine, Smith, & Lewis 1977; Pesch & Sanduleak 1983; Wasilewski 1983; Markarian, Lipovetskii, & Stepanian 1983; Zamorano *et al.* 1994; Popescu *et al.* 1996; Surace & Comte 1998; Ugryumov *et al.* 1999).

Despite their obvious advantages as detectors, CCDs were slow in replacing plates on Schmidt telescopes due to their small areal coverage. However, the availability of large-format CCDs in the early- and mid-1990s prompted many observatories to switch to the use of CCDs. This change in turn prompted a group of astronomers interested in extragalactic emission-line surveys to initiate a new CCD-based objective-prism survey. Called the KPNO

International Spectroscopic Survey (KISS), it is the first fully digital objective-prism survey for emission-line galaxies (ELGs).

The goal of KISS is to survey a substantial area of the sky (300–400 sq. deg.) to flux levels substantially deeper than previous photographic surveys. When completed, we expect to have cataloged roughly 5000 ELGs. Because of the great depth of the survey, we do not need to cover as much area as previous surveys to be able to generate large samples of active galaxies for subsequent study. For example, the Markarian survey covered roughly 15,000 sq. deg. and catalogued 1500 objects. In the first two red KISS catalogs we have detected 2157 objects in only 128 sq. deg. Another important factor is that, due to the digital nature of the survey data, the completeness characteristics and flux limits are readily measurable *from the survey data themselves*. Hence KISS is uniquely suited for a broad range of studies that require statistically complete samples of galaxies.

This is the fourth paper in the KISS series. The first

<sup>1</sup> Visiting Astronomer, Kitt Peak National Observatory, National Optical Astronomy Observatory, which is operated by the Association of Universities for Research in Astronomy, Inc. (AURA) under cooperative agreement with the National Science Foundation.

<sup>2</sup> present address: Department of Astronomy & Astrophysics, Pennsylvania State University, University Park, PA 16802; caryl@astro.psu.edu.

<sup>3</sup> present address: Astronomy Department, University of Florida, Gainesville, FL, 32611; vicki@astro.ufl.edu.

<sup>4</sup> present address: UCO/Lick Observatory, UC Santa Cruz, Santa Cruz, CA, 95064; laura@astro.ucsc.edu.

presents a complete description of the survey method, including a discussion of the survey data and its associated uncertainties (Salzer *et al.* 2000; hereafter Paper I). The first survey list of H $\alpha$ -selected ELGs, informally referred to as the red survey, is given in Salzer *et al.* (2001; hereafter KR1), while the first list of [O III]-selected galaxies (the blue survey) is found in Salzer *et al.* (2002; hereafter KB1). The current paper follows a format similar to KR1; for the sake of brevity, the reader is referred to Paper I and KR1 for many details. The observational data and image processing are described in Section 2, while the new list of ELG candidates is presented in Section 3. The properties of the new list of H $\alpha$ -selected ELGs are described in Section 4, while our results are summarized in Section 5.

## 2. OBSERVATIONS & REDUCTIONS

All survey data were acquired using the 0.61-meter Burrell Schmidt telescope<sup>5</sup>. The detector used for all data reported here was a  $2048 \times 4096$  pixel SiTe CCD. This CCD is not identical to the one used for the previous two survey lists, giving a different image scale and field-of-view. The CCD has  $15\text{-}\mu\text{m}$  pixels, yielding an image scale of  $1.43$  arcsec/pixel at the Newtonian focus of the telescope. The overall field-of-view was  $50 \times 100$  arcmin, and each image covered  $1.37$  square degrees. The long dimension of the CCD was oriented north-south during our survey observations. The red survey spectral data were obtained with a  $4^\circ$  prism, which provided a reciprocal dispersion of  $17 \text{ \AA}/\text{pixel}$  at H $\alpha$  with the new CCD. The spectral data were obtained through a special filter designed for the survey, which covered the spectral range  $6400 - 7200 \text{ \AA}$  (see Figure 1 of Paper I for the filter transmission curve).

The current survey was carried out in a strip at constant declination by observing a series of contiguous fields offset from each other in right ascension. The survey is centered at  $\delta(1950) = 43^\circ 30'$ , and each field covers  $100$  arcmin ( $1.6$  degrees) in the declination direction. The RA coverage of the survey strip is from  $11^h 55^m$  to  $16^h 15^m$ . The location of the strip was chosen to pass through the center of the Boötes Void (Kirshner *et al.* 1981, 1983, 1987). We selected this area of the sky because of our interest in the spatial distribution of galaxies in and around the void. Additionally, there have been a number of previous surveys that have looked at this region of the sky (Sanduleak & Pesch 1982, 1987; Moody *et al.* 1987; Aldering 1990), giving us a comparison sample of previous objective-prism-selected and line-selected galaxies.

As with our previous survey strips, we obtained images of each survey field both with and without the objective prism on the telescope. The images taken without the prism (referred to as direct images) were obtained through standard B and V filters. The direct images were photometrically calibrated, and provide accurate astrometry and photometry for all sources in the survey fields. We used uniform exposure times for all survey fields:  $4 \times 720$  s for the objective-prism (spectral) data, and  $2 \times 300$  s for V and  $1 \times 600$  s in B for the direct images. The telescope was dithered by a small amount ( $\sim 10$  arcsec) between exposures.

Table 1 lists the observing runs during which the current set of survey fields were observed. The first column gives the UT dates of the run, while the second column indicates the number of nights on which observations were obtained. At least some data were obtained on 26 of 27 scheduled nights (96%). The last two columns indicate the number of direct and spectral images, respectively, obtained during each run. It was common practice to observe in both direct and spectral modes during parts of each run, although it was not always the case that the direct and spectral images of a given field were obtained during the same run.

All data reduction took place using the Image Reduction and Analysis Facility (IRAF<sup>6</sup>) software. A special package of IRAF-based routines that were written by members of the KISS team was used for most of the data analysis. Full details of the observing procedures and data reduction methods are given in Paper I and KR1.

## 3. LIST 2 OF THE KPNO INTERNATIONAL SPECTROSCOPIC SURVEY

### 3.1. Selection Criteria

The selection of the second red (H $\alpha$ ) list of ELG candidates was carried out in precisely the same fashion as the original red list (KR1). Full details are presented in Paper I and KR1. To briefly summarize, we use our automated KISS software to evaluate the extracted objective-prism spectrum of each object located within a survey field. All objects with spectral features that rise more than five times the local noise above the continuum level are flagged as potential ELGs. This  $5\sigma$  threshold is the primary selection criterion of the survey, and was arrived at after substantial testing during the early phases of the KISS project. Following the initial automated selection, all candidates are visually examined, and spurious sources are removed from the sample. Finally, the objective-prism images are scanned visually for sources that might have been missed by the software. These tend to be objects where the emission line is redshifted to the red end of the objective-prism spectrum, so that the software cannot detect continuum on both sides of the line. The combination of our automated selection process and our careful visual checking helps to ensure a high degree of reliability that the KISS ELG candidates are real, and that the sample is largely complete for all objects with  $5\sigma$  emission lines.

As described in KR1, we also flag objects that have emission lines between  $4\sigma$  and  $5\sigma$  during our selection process. These  $4\sigma$  detections represent objects with somewhat weaker emission lines than the main KISS sample, but they are nonetheless valid ELG candidates and likely include a number of interesting sources. However, these objects do not constitute a statistically complete sample in the same sense as the main ( $> 5\sigma$ ) list. We report the  $4\text{-}5\sigma$  sources in a secondary list of ELG candidates (see Appendix), which should be thought of as a supplement to the main KISS catalog.

### 3.2. The Survey

<sup>5</sup> Observations made with the Burrell Schmidt telescope of the Warner and Swasey Observatory, Case Western Reserve University.

<sup>6</sup> IRAF is distributed by the National Optical Astronomy Observatory, which is operated by the Association of Universities for Research in Astronomy, Inc., (AURA) under cooperative agreement with the National Science Foundation.

The list of ELG candidates selected in the second red survey is presented in Table 2. Because the survey data includes both spectral images and photometrically-calibrated direct images, we are able to include a great deal of useful information about each source, such as accurate photometry and astrometry and estimates of the redshift, emission-line flux and equivalent width. Only the first page of the table is printed here; the complete table is available in the electronic version of this paper.

The contents of the survey table are as follows. Column 1 gives a running number for each object in the survey with the designation KISSR *xxxx*, where KISSR stands for “KISS red” survey. This is to distinguish it from the blue KISS survey (KB1). The KR1 survey list included KISSR objects 1–1128, and here we present KISSR objects 1129–2157. Columns 2 and 3 give the object identification from the KISS database tables, where the first number indicates the survey field (*Fxxxx*), and the second number is the identification number within the table for that galaxy. This identifier is necessary for locating the KISS ELGs within the survey database tables. Columns 4 and 5 list the right ascension and declination of each object (J2000). The formal uncertainties in the coordinates are 0.25 arcsec in RA and 0.20 arcsec in declination. Column 6 gives the B magnitude, while column 7 lists the B–V color. For brighter objects, the magnitude estimates typically have uncertainties of 0.05 mag, increasing to  $\sim 0.10$  mag at B = 20. Paper I includes a complete discussion of the precision of both the astrometry and photometry of the KISS objects. An estimate of the redshift of each galaxy, based on its objective-prism spectrum, is given in column 8. This estimate assumes that the emission line seen in the objective-prism spectrum is H $\alpha$ . Follow-up spectra for >1200 ELG candidates from the two red survey lists (KR1 and the current list) show that this assumption is correct in the vast majority of cases. Only 35 ELGs with follow-up spectra (2.8%) are high redshift objects where a different line (typically [O III] and/or H $\beta$ ) appears in the objective-prism spectrum. Nine objects in the table have negative redshifts, although only two of these are more than  $1\sigma$  below 0.0000. We have obtained follow-up spectra for four of the nine: three are high redshift objects where the detected line is not H $\alpha$ , and one is a low-*z* star-forming galaxy with an actual redshift of 0.0006. The formal uncertainty in the redshift estimates is  $\sigma_z = 0.0028$  (see Section 4.1.3). Columns 9 and 10 list the emission-line flux (in units of  $10^{-16}$  erg/s/cm<sup>2</sup>) and equivalent width (in Å) measured from the objective-prism spectra. The calibration of the fluxes is discussed in section 4.1.2. These quantities should be taken as being representative estimates only. A simple estimate of the reliability of each source, the quality flag (QFLAG), is given in column 11. This quantity, assigned during the line measurement step of the data processing, is given the value of 1 for high quality sources, 2 for lower quality but still reliable objects, and 3 for somewhat less reliable sources. Column 12 gives alternate identifications for KISS ELGs which have been cataloged previously. This is not an exhaustive cross-referencing, but focuses on previous objective-prism surveys which overlap part or all of the current survey area: Markarian (1967) and Case (Pesch & Sanduleak 1983). Also included are objects in common with the *Uppsala General Catalogue of Galaxies*

(UGC, Nilson 1973).

A total of 1029 ELG candidates are included in this second list of H $\alpha$ -selected KISS galaxies. The total area covered by the second red survey strip is 65.8 deg<sup>2</sup>, meaning that there are 15.6 KISS ELGs per square degree. For the first and second red lists combined, the surface density is 16.9 galaxies deg<sup>-2</sup>. This compares to the surface density of 0.1 galaxies deg<sup>-2</sup> from the Markarian survey, and 0.56 galaxies per deg<sup>2</sup> from the UCM survey; the present survey is much deeper! The second red survey strip has a somewhat lower surface density than the first red survey strip. This could be an effect of the Boötes void, which is included in the area covered by the second survey strip.

Of the 1029 objects cataloged, 630 were assigned quality values of QFLAG = 1 (61.2%), 318 have QFLAG = 2 (30.9%), and 81 have QFLAG = 3 (7.9%). Based on our follow-up spectra to date, 98.6% (206 of 209) of the sources with QFLAG = 1 are *bona fide* emission-line galaxies, compared to 81.5% (66 of 81) with QFLAG = 2 and 64.7% (11 of 17) with QFLAG = 3. Overall, 92.2% of the objects with follow-up spectra are *bona fide* ELGs. The properties of the KISS galaxy sample are described in the next section.

Figure 1 shows an example of the finder charts for the KISS ELGs. These are generated from the direct images obtained as part of the survey, and represent a composite of the B- and V-band images. Figure 2 displays the extracted spectra derived from the objective-prism images for the first 24 ELGs in Table 1. Finder charts and spectral plots for all 1029 objects in the current survey list are available in the electronic version of this paper.

A supplementary table containing an additional 291 ELG candidates is included in the appendix of this paper (Table 4). These galaxies are considered to be lower probability candidates, having emission lines with strengths between  $4\sigma$  and  $5\sigma$ . These additional galaxies do not constitute a statistically complete sample, and should therefore be used with caution. However, there are likely many interesting objects contained in this supplementary list. Hence, following the precedent established in KR1, we list these objects in order to give a full accounting of the ELGs in the area surveyed.

#### 4. PROPERTIES OF THE KISS ELGS

The survey method employed by KISS makes it possible to obtain a general picture of the survey constituents, even in the absence of follow-up observations. A large amount of information is available for each ELG candidate from the survey data themselves. Accurate B and V photometry, astrometry, and morphological data can be derived from the direct images, and the digital objective-prism spectra allow us to measure line strengths and positions. However, due to the low resolution and limited spectral range of the objective-prism spectra, it is not possible to distinguish between different types of galactic activity based on the survey data alone. Follow-up spectroscopy is necessary to develop a more complete understanding of the nature of each ELG. In the following section, we use the survey data to investigate the key properties of the second H $\alpha$ -selected KISS ELG sample.

##### 4.1. Observed Properties

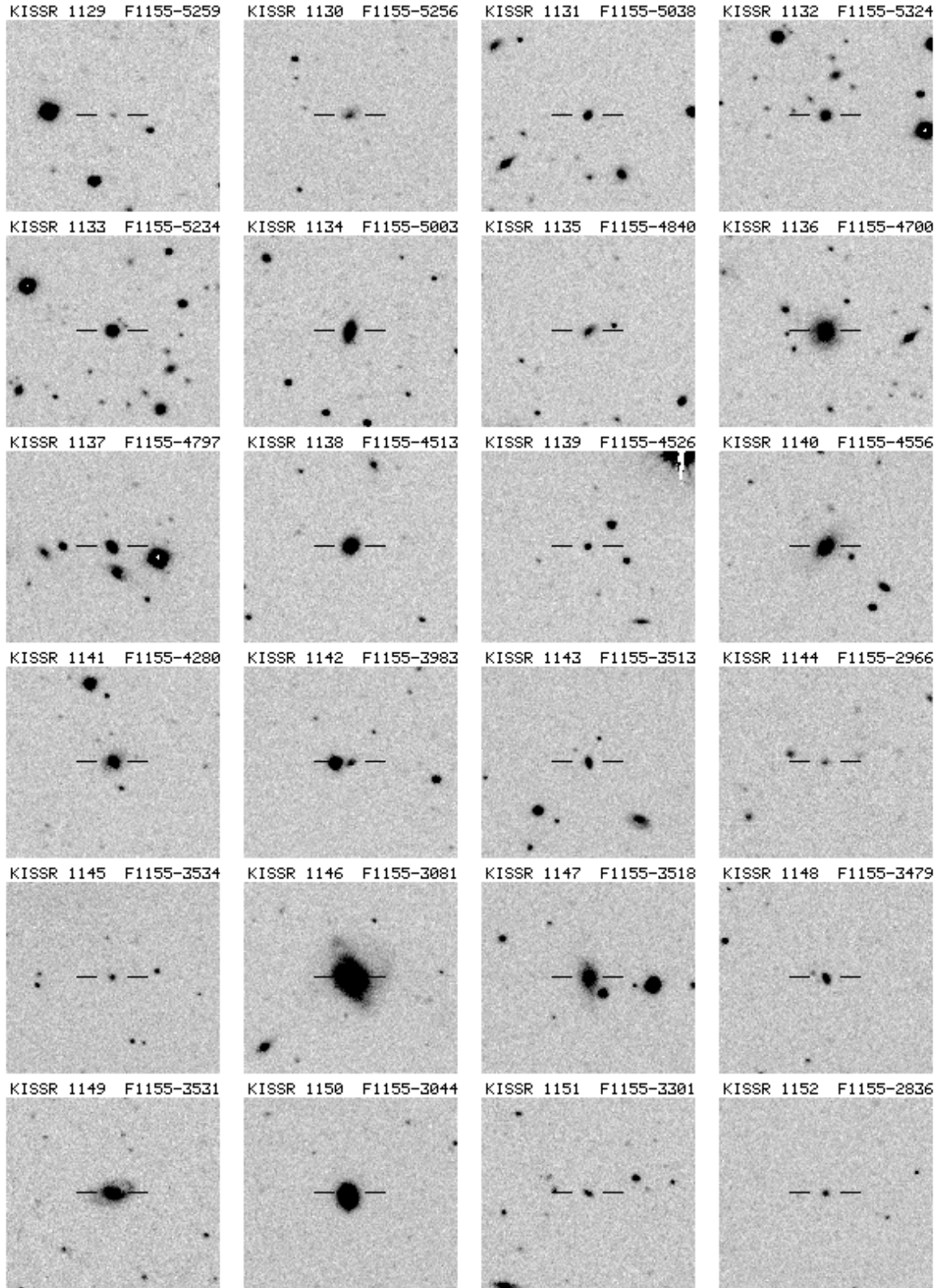


FIG. 1.— Example of finder charts for the KISS ELG candidates. Each image is  $3.2 \times 2.9$  arcmin, with N up, E left. These finders are created from a composite of the B- and V-band direct images obtained as part of the survey. In all cases the ELG candidate is located in the center of the image section displayed, and is indicated by the tick marks.

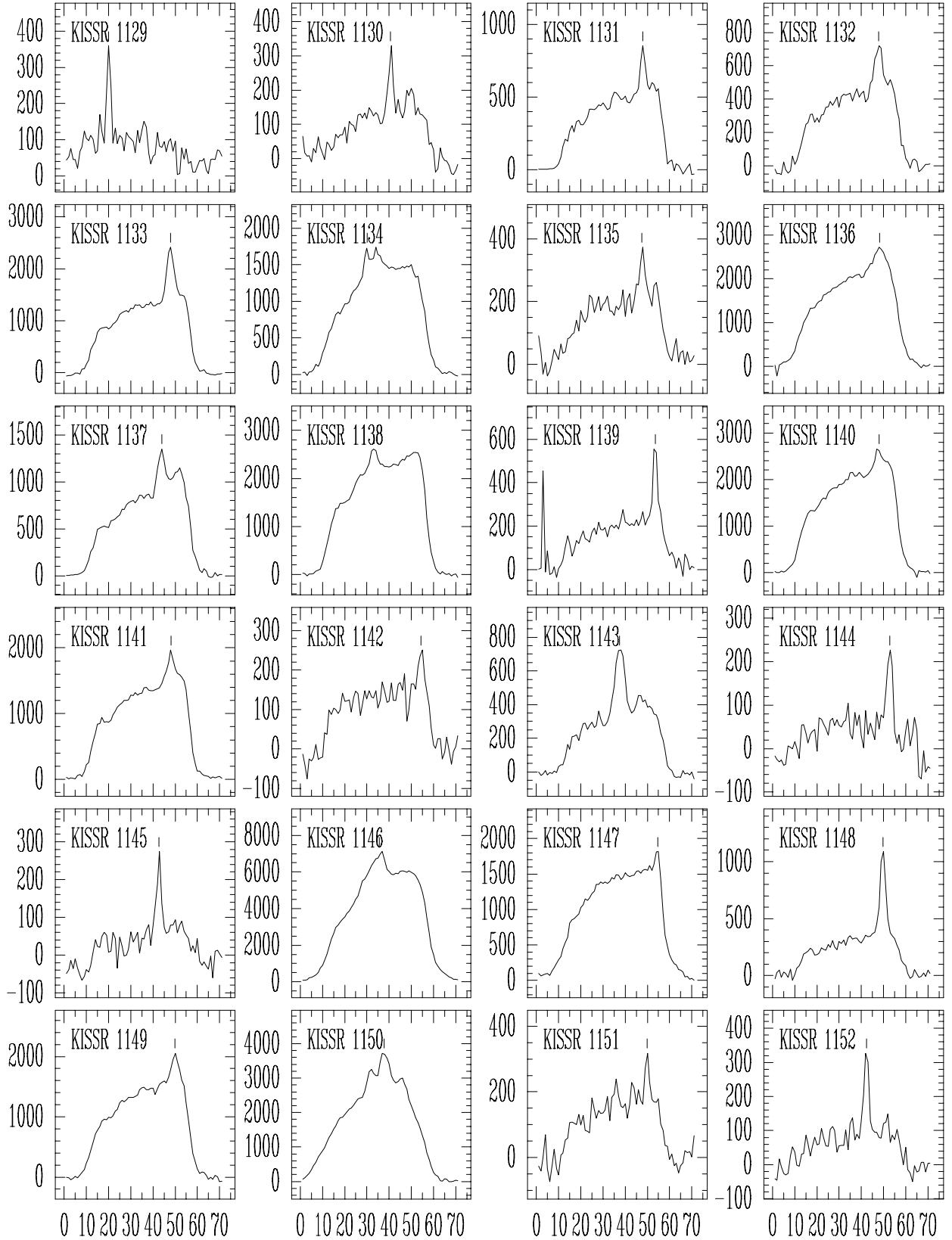


FIG. 2.— Plots of the objective-prism spectra for 24 KISS ELG candidates. The spectral information displayed represents the extracted spectra present in the KISS database tables. The location of the putative emission line is indicated.

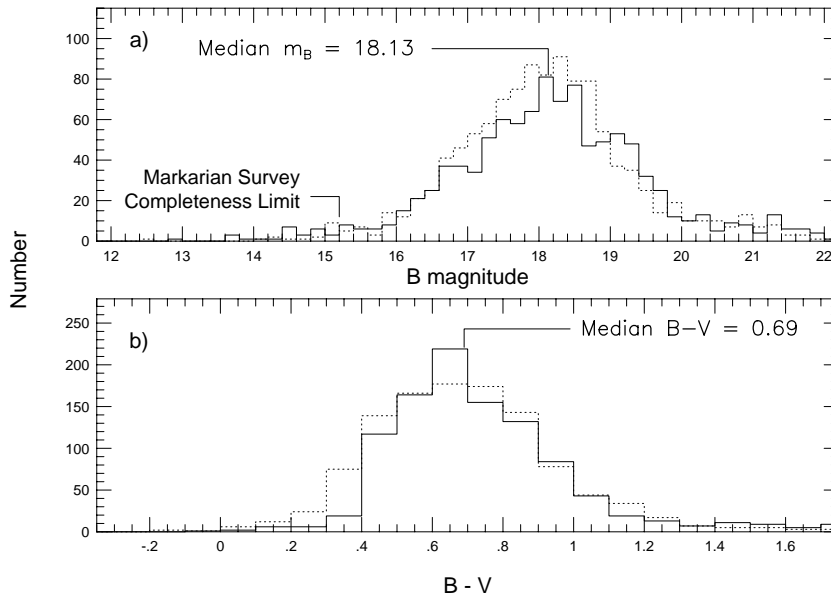


FIG. 3.— (a) Distribution of B-band apparent magnitudes for the 1029 ELG candidates in the second  $H\alpha$ -selected KISS survey list. The median brightness in the KISS sample is  $B = 18.13$ , with 8% of the galaxies having  $B > 20$ . Also indicated, for comparison, is the completeness limit of the Markarian survey. (b) Histogram of the  $B-V$  colors for the 1029 ELG candidates. The median color of 0.69 is indicated. The dotted lines show the magnitude and color distributions of the ELG candidates in the first KISS survey list.

#### 4.1.1. Magnitude & Color Distributions

Figure 3a plots the B-band apparent magnitude distribution for the 1029 KISS ELGs in the second red survey list, while Figure 3b displays the distribution of  $B-V$  colors. The median values of both apparent magnitude and color are indicated. For comparison, the histogram for the first red survey list is shown in this and the following figures as a dotted line.

The median apparent B magnitude of the second survey list is 18.13. This value is very close to that of the first red survey list, which has a median apparent magnitude of  $B = 18.08$ . This compares to median apparent magnitudes of  $B = 16.9$  for the  $[O\ III]$ -selected Michigan (UM) survey (Salzer *et al.* 1989) and  $B \approx 16.1$  for the  $H\alpha$ -selected UCM survey (Pérez-González *et al.* 2000). The completeness limit of the Markarian survey,  $B = 15.2$  (Mazzarella & Balzano 1986) is indicated in Figure 3a. The KISS sample clearly probes substantially deeper than previous objective-prism surveys.

The median color of the second red survey list is  $B-V = 0.69$ , which is nearly identical to the median color of the first red survey list,  $B-V = 0.67$ . Both of these median values fall in the typical color range of an Sb galaxy (Roberts & Haynes 1994). The color distribution appears to be similar to that of the UCM galaxies (Pérez-González *et al.* 2000), which have a mean  $B-r$  color of 0.71. This mean value is comparable to the mean color of an Sbc galaxy (Fukugita *et al.* 1995). The KISS red survey and the UCM survey galaxies are both significantly redder than the KISS blue survey (median color of  $B-V = 0.50$ ; KB1), or the UM survey (median color of 0.54; Salzer *et al.* 1989). The reason for this difference can be found in the selection methods of the surveys. The UM and KB1 surveys are both  $[O\ III]$ -selected, hence they preferentially detected

ELGs with lower luminosities and with low amounts of reddening. In contrast,  $H\alpha$ -selected surveys tend to detect a larger proportion of more luminous starburst galaxies and AGN, and they are significantly less biased against heavily reddened ELGs. In addition to these intrinsically red and/or higher reddening galaxies, the  $H\alpha$ -selected KISS sample also contains a large number of dwarf galaxies (see Section 4.2.1). Hence it exhibits a color range that more closely matches that of the overall galaxian population.

The color distribution shows an extended tail of very red ELGs. A total of 62 KISS galaxies in the current list possess  $B-V$  colors  $> 1.2$  (i.e., redder than any unreddened stellar population typical of a normal galaxy). The median apparent magnitude of these red objects is  $B = 20.7$ . At such faint magnitudes the uncertainties in the photometry are substantial (typical errors in the  $B-V$  color are 0.2 to 0.3 magnitude). Spectroscopic follow-up observations have been obtained for nine of these very red ELG candidates, and only three have been confirmed as ELGs. The remaining six are stars or faint galaxies with no emission lines. These results indicate that many of these faint, red candidates are probably false detections; the proportion of spurious sources is known to increase at fainter magnitudes. This is reflected in the fact that 89% of these red objects (55 of 62) were assigned quality codes of 2 or 3. However, all three of the confirmed red ELGs mentioned above are Seyfert galaxies, which suggests that follow-up spectra will reveal some interesting objects in this population of very red KISS objects.

#### 4.1.2. Line Strength Distributions and Survey Completeness

The digital nature of the survey data, along with our KISS software, allow us to measure the position and

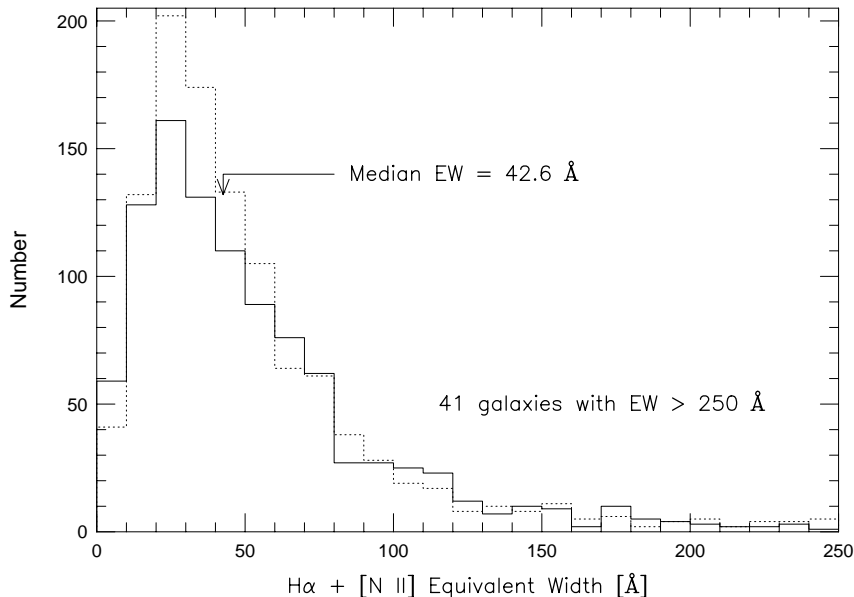


FIG. 4.— Distribution of measured  $H\alpha + [N II]$  equivalent widths for the KISS ELGs. The median value of  $42.6 \text{ \AA}$  is indicated. The measurement of equivalent widths from objective-prism spectra tends to yield underestimates of the true equivalent widths, so these values should be taken only as estimates. The survey appears to detect most sources with  $EW(H\alpha+[N II]) > 20\text{--}30 \text{ \AA}$ . The dotted line shows the equivalent width distribution of the ELG candidates in the first KISS survey list.

strength of the emission lines that are seen in the objective-prism spectra of the KISS candidates. We are able to measure both the emission line flux and equivalent width for each source, which allows us to utilize the survey data themselves to investigate issues like the star-formation rate density in the local universe. In addition, we are able to assess the completeness of our ELG sample directly from the survey data. Since KISS is a line-selected survey, its completeness limit must be defined in terms of line strengths, not continuum apparent magnitudes (Salzer 1989). Gronwall *et al.* (2004) describes our method for determining the completeness of the survey and derives an estimate of the local star-formation rate density, using the KR1 sample.

For the reasons discussed in KR1, we do not expect our measured line strengths to be as precise as those obtained from slit spectra. In particular, equivalent widths measured from extended sources will tend to be underestimated due to the slitless nature of the objective-prism spectra. Since continuum light from many portions of the galaxy can be dispersed by the prism to the location of the emission line in the objective-prism spectrum, this effect can be large, leading to underestimates of factors of two or more in the survey equivalent widths! Wegner *et al.* (2003) presents a thorough comparison of the equivalent widths measured from both the survey data and slit spectra for over three hundred KISS ELGs. On the other hand, we expect that our measured line *fluxes* should be more representative of the total emission from our galaxies than will fluxes measured from slit spectra, especially for extended objects. This is because we sum over 5 pixels (7.3 arcsec) when we extract the objective-prism spectra, compared to a typical slit width of 1 – 2 arcsec for our follow-up spectra. Furthermore, the field-to-field flux calibration employed (Paper I) ensures that the entire survey is on precisely the

same relative flux scale. Thus, the KISS line fluxes should represent fairly accurate estimates of the total  $H\alpha + [N II]$  emission.

We display the distribution of equivalent widths seen in our survey galaxies in Figure 4. Since we are without the benefit of follow-up spectra for the majority of our candidates, we must assume that the line we are measuring is  $H\alpha + [N II]$ . Based on our follow-up spectra to date (see Section 3.2), this appears to be a reasonable assumption. The  $[N II]\lambda\lambda 6584, 6548$  lines are always blended with  $H\alpha$  at our spectral resolution; there is no way to determine the contribution from the individual lines using our survey data. However, the  $[S II]\lambda\lambda 6731, 6717$  doublet is well resolved from the  $H\alpha + [N II]$  complex, and is often seen in the objective prism spectra of strong-lined objects. The median equivalent width found from the current sample of ELGs is  $42.6 \text{ \AA}$ . This agrees closely with the median equivalent width of the first survey list, which is  $41.0 \text{ \AA}$ . The vast majority of the galaxies have equivalent widths less than  $100 \text{ \AA}$ . The distribution of EWs peaks in the  $20\text{--}30 \text{ \AA}$  bin, suggesting that KISS is fairly complete for objects with EWs above  $\sim 30 \text{ \AA}$ .

The calibration of the flux scale is a two-step process. First, the objective-prism spectra for each field are corrected for throughput variations and atmospheric extinction. This places all line fluxes on the same *relative* flux scale. Then, the fluxes are calibrated using information obtained from our follow-up spectra. At the time of this writing, we have obtained slit spectra for 307 KISS candidates from the sample of 1029 presented in this paper. From these, we select galaxies that are starforming (i.e., not AGN), are of high quality, and had been observed with a long-slit spectrograph under photometric conditions. Galaxies observed through optical fibers were not

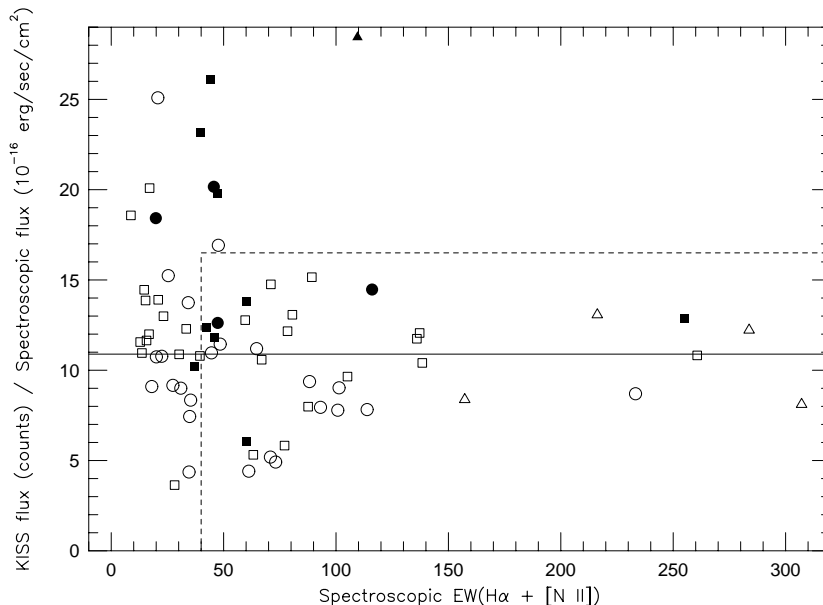


FIG. 5.— Plot of the ratio of objective-prism flux (in counts) to spectroscopic flux *versus*  $H\alpha + [N II]$  equivalent width measured from the follow-up spectra. Data from six different observing runs on three different telescopes are plotted: open square = MDM 2.4-m in May, 2000, open circle = KPNO 2.1-m in July 2000, open triangle = Lick 3.0-m in April, 2001, filled square = MDM 2.4-m in April, 2002, filled triangle = Lick 3.0-m in April, 2002, and filled circle = MDM 2.4-m in April, 2003. The solid line indicates the median ratio. The dashed lines show the criteria we applied to select the calibration sample. Four galaxies with flux ratios  $> 30$  fall above the diagram, and one galaxy with  $EW > 320 \text{ \AA}$  lies off the diagram to the right.

used, since such spectra are notoriously difficult to use for accurate spectrophotometry. This limited our calibration sample to 75 galaxies. All data used were obtained using slit widths of either 1.7 or 2.0 arcsec. These wide slits guarantee that we recorded most of the emission-line flux from the sources, as long as the emission regions were not spatially extended. Since the fluxes measured from the objective-prism spectra are a combination of the  $H\alpha$  and  $[N II]$  lines, we used the fluxes from our slit spectra for the sum of these three lines. Figure 5 shows a plot of the ratio of objective-prism flux (in counts) to spectroscopic flux *versus* the equivalent width measured from the follow-up spectra. Data from six different observing runs on three different telescopes are plotted, and there are no obvious systematic trends in this ratio with either equivalent width or observing run. There are, however, a number of galaxies with large ratios, particularly at low equivalent width. A visual inspection of the survey images showed that these galaxies are of large angular extent and exhibit extended line emission. The high flux ratios for these objects indicate that our long-slit measurements do not include all of the  $H\alpha$  emission from these sources. Thus, we restricted our analysis to those galaxies with an objective-prism-to-spectroscopic flux ratio of less than 16.5 and an equivalent width greater than  $40 \text{ \AA}$ , leaving us with a calibration sample of 38 galaxies. These galaxies all possess emission regions that are essentially point sources. The median flux ratio of this sample was 10.89; the mean was 10.25 with a standard deviation of 2.96 and an error in the mean of 0.48. We have adopted as our calibration value the reciprocal of the median value, or  $0.0918 \times 10^{-16} \text{ ergs/sec/cm}^{-2}$  per count.

This calibration value is applied to our measured

objective-prism line fluxes to convert their instrumental fluxes (in counts) to calibrated fluxes (in  $\text{erg/s/cm}^2$ ). The distribution of observed  $H\alpha + [N II]$  line flux values for the 1029 KISS ELGs is displayed in Figure 6. The median value of  $7.7 \times 10^{-15} \text{ erg/s/cm}^2$  is somewhat lower than the first survey list median flux of  $8.7 \times 10^{-15} \text{ erg/s/cm}^2$ . This suggests that the data used for the current survey list are slightly more sensitive than those used for KR1, which is likely due to the improved pixel scale and hence better spectral resolution achieved with the new CCD. For comparison, the median flux from the UCM sample is  $2.9 \times 10^{-14} \text{ erg/s/cm}^2$  (based on follow-up spectra of Gallego *et al.* 1996). A galaxy with this latter flux level would fall at the extreme right edge of the figure, which illustrates the increased depth of KISS relative to the UCM survey in terms of line flux.

The calibrated line fluxes are used to determine the completeness limit of the survey. Using the procedure described in Gronwall *et al.* (2004), we convert these fluxes into pseudo-magnitudes – the line magnitude  $m_L$ . We then apply a  $V/V_{max}$  analysis (e.g., Schmidt 1968, Huchra & Sargent 1973) to the full sample of 1029 galaxies. The results are shown in Table 3. The contents of the table are as follows: Column (1) lists  $m_{comp}$ , the value of  $m_L$  for which  $\langle V/V_{max} \rangle$  is being computed. Column (2) lists the total number of ELGs brighter than that  $m_L$  level, while columns (3) and (4) gives the numbers of objects in the volume-limited and flux-limited subsamples, respectively. Note that some objects may start out in the flux-limited sample at brighter values of  $m_{comp}$ , then move into the volume-limited sample at fainter values of  $m_{comp}$ . Column (5) lists the mean  $V/V_{max}$  for the flux-limited subsample. Column (6) shows the number of galaxies that need to



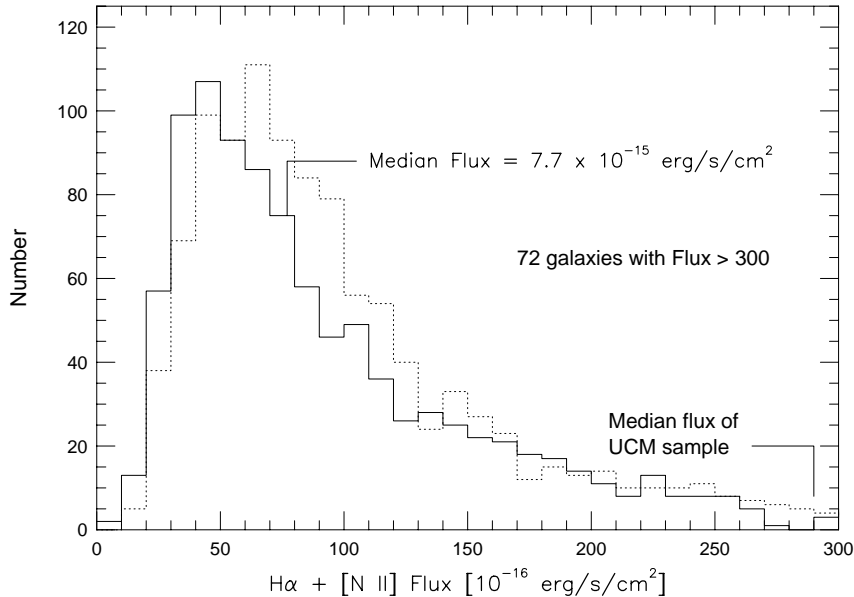


FIG. 6.— Distribution of  $H\alpha + [N II]$  line fluxes for the 1029 KISS ELGs included in the current survey list. The median flux level of both the KISS and UCM samples is indicated. The dotted line shows the line flux distribution of the ELG candidates in the first KISS survey list.

be added to the sample at each  $m_{comp}$  level to maintain  $\langle V/V_{max} \rangle = 0.5$ , and column (7) lists the cumulative number of galaxies added at all magnitudes brighter than the given magnitude level to maintain  $\langle V/V_{max} \rangle$ . Column (8) shows the percentage of objects that are in the flux-limited subsample, which decreases continuously as  $m_L$  becomes fainter. Column (9) lists the completeness percentage of the flux-limited subsample as a function of  $m_L$ . These latter two quantities are plotted in Figure 7.

The interpretation of the  $V/V_{max}$  test follows exactly the discussion found in Gronwall *et al.* (2004) for the KR1 sample, and hence will not be repeated here. Rather, we will simply summarize the main results. First, we note that because of the redshift limit imposed by the filter used for the survey, objects in the sample can be either line-flux-limited or volume-limited objects, depending on the strength of their  $H\alpha + [N II]$  emission and their actual redshift. As the limiting line flux (parameterized by  $m_L$ ) decreases, a given object can actually switch from being in the flux-limited category to the volume-limited category. For faint limiting line fluxes (fainter  $m_L$ ) the majority of the KISS ELGs are in the volume-limited subsample. This is illustrated by the dashed line in Figure 7. Second, we see that the KISS sample is 100% complete down to  $m_L = 15.5$ , which is nearly identical to the result for the KR1 sample (Gronwall *et al.* 2004). This completeness limit includes 630 KISS ELGs, or 61.2% of the sample. One can construct a “correctably complete” sample by extending the line-flux limit down to even lower values. For example, at  $m_L = 16.2$ , the sample is still 73.6% complete, but now includes 89.7% of the sample.

#### 4.1.3. Redshift Distributions

Another parameter that we derive from the objective-prism spectra is the redshift of each object. Following

the example from Paper I, we can compare the objective-prism redshifts obtained from the survey data with redshifts derived from slit spectra for those objects for which follow-up spectra have been obtained. This allows us to assess the uncertainty associated with the objective-prism redshifts. Figure 8 plots  $z_{KISS}$  (objective-prism redshift) against  $z_{spec}$  (follow-up spectra redshifts), and in general shows excellent agreement between the two measurements. A few objects deviate substantially from the equality line. We checked several such objects in the original survey data and discovered that, in all cases, the emission region is offset from the center of the galaxy in a north-south direction. Because the dispersion of the objective-prism spectra is in the N-S direction, and because of the slitless nature of the spectra and the manner in which they are extracted (see Paper I), objects with emission regions that are off-center will yield unreliable redshift estimates from their objective-prism spectra. This is the case for only a small minority of KISS objects. The RMS scatter of  $z_{KISS}$  about the equality line is  $0.0036$  ( $1080 \text{ km s}^{-1}$ ). However, if the three most deviant objects are removed from the diagram, the RMS scatter is reduced to  $0.0028$  ( $840 \text{ km s}^{-1}$ ). We adopt this latter value as our redshift precision. It is precisely the same value found for the KR1 sample (Paper I).

For objects in the KR1 survey list it was necessary to apply a correction to objective-prism redshifts above  $z = 0.07$  (the details are given in Paper I). Above this redshift, the value of  $z_{KISS}$  systematically underestimated the true redshift because the  $H\alpha$  line begins to redshift out of the survey bandpass. However, the objects plotted in Figure 8 do not display this offset: the objective-prism redshifts agree well with redshifts determined from follow-up spectroscopy out to the  $z \sim 0.1$  cutoff imposed by the survey filter. The reason for this difference is probably the better pixel scale

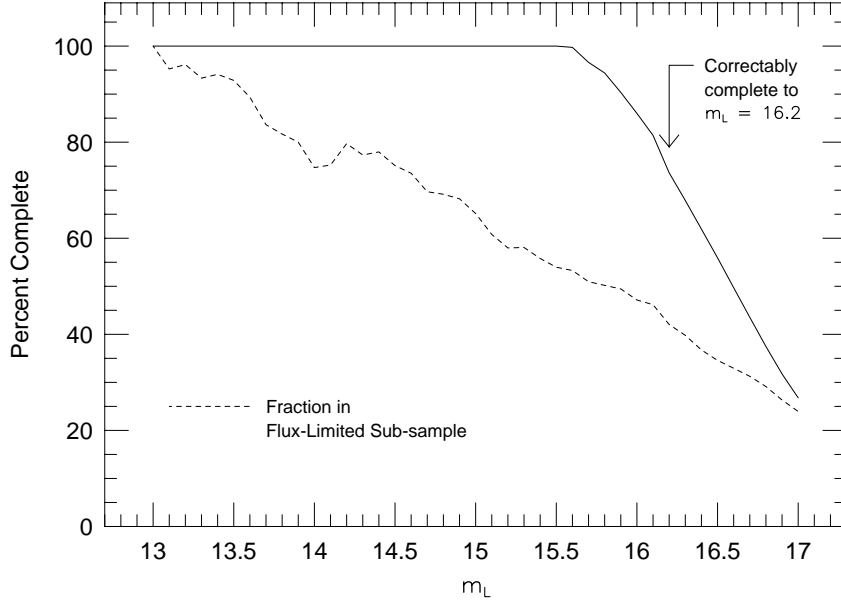


FIG. 7.— Plot of the completeness percentage as a function of  $m_L$  for the current sample (solid line). The catalog is 100% complete to  $m_L = 15.5$ , and is “correctably complete” to  $m_L = 16.2$ . The dashed line shows the fraction of the sample contained in the flux-limited sub-sample as a function of  $m_L$ . At the completeness limit, roughly half of the KISS ELGs are in the flux-limited portion of the sample.

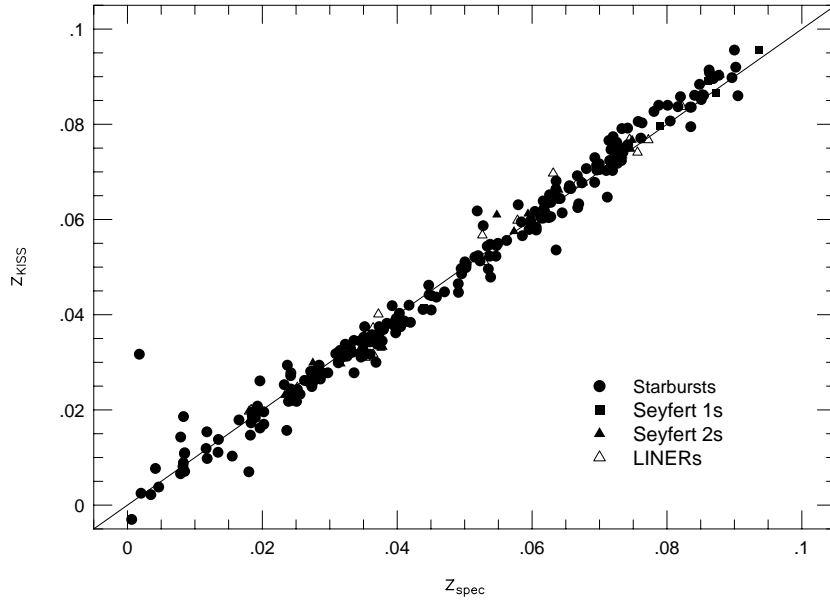


FIG. 8.— Comparison between objective-prism redshifts ( $z_{KISS}$ ) obtained from our survey data and slit-spectra redshifts ( $z_{spec}$ ) obtained from follow-up spectra. The solid line denotes  $z_{KISS} = z_{spec}$ . The objective-prism redshifts provide reasonable estimates of the true redshifts over the full range covered by the survey. The formal uncertainty in  $z_{KISS}$  is  $0.0028$  ( $840 \text{ km s}^{-1}$ ).

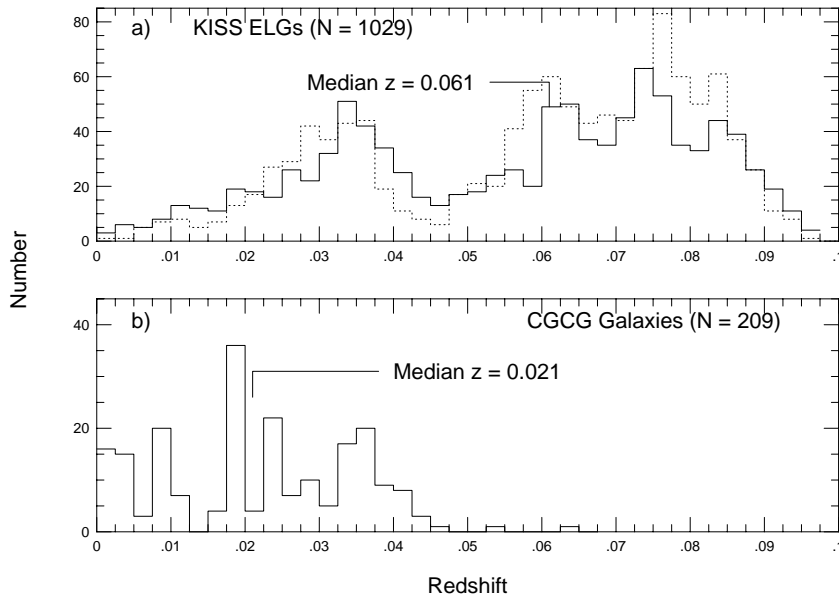


FIG. 9.— Histograms showing the distribution of redshift for (a) the 1029 H $\alpha$ -selected KISS ELGs and (b) the 209 “normal” galaxies from the CGCG that are located in the same area of the sky. The dotted line in the top panel shows the redshift distribution of the ELG candidates in the first KISS survey list. The median redshift is indicated in both plots. Note that the number of KISS ELGs continues to rise up to the cut-off of the filter used for the survey, indicating that the survey is volume-limited for the more luminous galaxies. The deficit of ELGs between  $z = 0.04$  and  $0.06$  is due to the Boötes void.

of the CCD used for the second red survey. We do not apply any corrections to the objective-prism redshifts listed in Table 2

Figure 9 illustrates the distribution of the objective-prism redshifts. The upper panel shows the redshift distribution of the KISS ELGs from the second red survey list as a solid line, and the distribution of the first red survey list is indicated by a dotted line. The lower panel shows the redshift distribution for a comparison sample of galaxies from Zwicky *et al.* (1961–1968; hereafter CGCG). The redshifts for the 209 CGCG galaxies are taken from Falco *et al.* (1999); this is essentially the portion of the CfA2 redshift survey that covers the same area on the sky as the KISS ELGs. The Falco *et al.* redshift catalog sample is complete to  $m_B = 15.5$ . Because the surface density of the CGCG catalog is fairly low, we included objects lying in a four-degree-wide declination strip, rather than the 1.6 degree covered by KISS. We use these CGCG galaxies as our comparison sample in the following section as well.

From Figure 9 it is immediately apparent that KISS detects large numbers of galaxies to much higher redshifts than what is found in the CGCG sample. The median redshift for the KISS sample is nearly three times greater than that of the magnitude-limited CGCG galaxies. The Boötes void is the reason for the large drop in the number of galaxies between  $z = 0.04$  and  $0.06$  (see also Figure 12). Only a handful of CGCG galaxies are found beyond this void. In contrast, the number of KISS ELGs increases again beyond the Boötes void, out to the redshift limit imposed by the survey filter. The implications of this are (1) that the survey technique employed by KISS would be sensitive to galaxies at distances well beyond the distance limit imposed by the filter, if the filter was either not used or was replaced with one that extended to red-

der wavelengths, and (2) for the high-luminosity portion of the ELG luminosity function, the KISS sample is effectively volume-limited rather than flux-limited.

Comparison of the velocity histograms of the two KISS lists (Figure 9a) shows that they are very similar. In particular, the KR1 histogram shows a depression in the number of galaxies at velocities comparable to the Boötes void ( $12,000 - 18,000 \text{ km s}^{-1}$ ). While this may appear strange at first sight, since the two survey strips are separated by  $14^\circ$  in declination, the underdensity associated with the Boötes void is in fact quite large. For example, the original paper announcing the discovery of the void (Kirshner *et al.* 1981) was based on redshift survey data separated by  $43^\circ$  in declination ( $26^\circ$  to  $69^\circ$ ). Hence, the similarities in the two histograms is most likely indicating the linkage in the large-scale spatial distribution of the galaxies in these two widely separated fields.

## 4.2. Derived Properties

### 4.2.1. Luminosity Distribution

Using the redshifts and apparent magnitudes listed in Table 2 and assuming a value for the Hubble Constant of  $H_0 = 75 \text{ km/s/Mpc}$ , we compute absolute magnitudes for the second red survey list. Corrections for Galactic absorption ( $A_B$ ) have been applied by averaging the absorption values for all KISS emission-line galaxies in each survey field. The extinction value for each ELG position was extracted from the maps of dust infrared emission constructed by Schlegel, Finkbeiner, & Davis (1998). Since the majority of the survey strip is at high Galactic latitude, this correction is typically small: 55 of the 62 fields (89%) have  $A_B < 0.10$ , and all fields have  $A_B < 0.13$ . The maximum correction of  $A_B = 0.123$  occurs in one of the

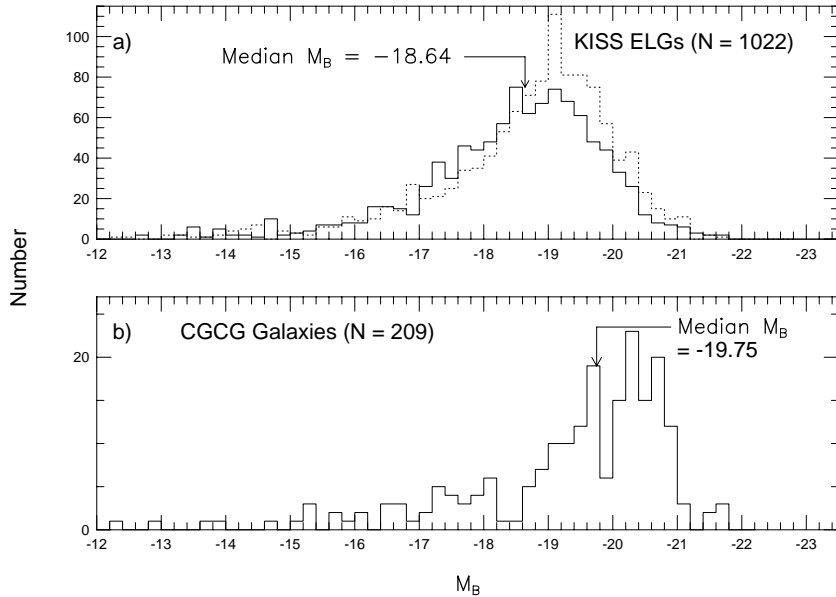


FIG. 10.— Histograms showing the distribution of blue absolute magnitude for (a) the 1029  $H\alpha$ -selected KISS ELGs and (b) the 209 “normal” galaxies from the CGCG that are located in the same area of the sky. The dotted line shows the luminosity distribution of the ELG candidates in the first KISS survey list. The median luminosity of each sample is indicated. The KISS ELG sample is made up of predominantly intermediate- and lower-luminosity galaxies, making this line-selected sample particularly powerful for studying dwarf galaxies.

easternmost survey fields (F1532). Note also that the large redshift uncertainties associated with the objective-prism spectra (Section 4.1.3) translate into significant uncertainties in our computed absolute magnitudes. For example, an object with the median redshift ( $z = 0.061$ ) will have an uncertainty in its  $M_B$  of 0.10 magnitude due to the redshift uncertainty alone. The error is much larger for nearby objects ( $\sim 0.4$  magnitude for a galaxy with  $z = 0.01$ ). These uncertainties should be kept in mind when interpreting Figure 10.

We compare the luminosities of the KISS ELGs with those of the CGCG galaxies located in the same area of the sky in Figure 10. The median blue absolute magnitude of the KISS ELGs is  $-18.64$ , which is roughly one magnitude fainter than  $M^*$ , the “characteristic luminosity” parameter of the Schechter (1976) luminosity function. As seen in the lower portion of the figure, the majority of the CGCG galaxies are more luminous than the KISS ELGs. The median absolute magnitude of the CGCG sample is  $-19.75$  (i.e., very close to  $M^*$ ).

We note that in this survey region, both the KISS sample and the CGCG samples have median luminosities that are roughly one-third of a magnitude fainter than those of the corresponding samples in the KR1 survey strip. This could be due to the fact that the second red survey strip runs through the center of the Boötes void. Since KR1 and the current survey list have comparable depths and similar velocity cutoffs, the main difference between them would appear to be a deficiency of galaxies at intermediate redshifts caused by the void. This could explain the differences in the median luminosities as due to the fact that the median and high luminosity objects that would naturally be visible at the distance of the void are “missing” from the sample. However, as noted above, KR1 has

a similar depression in its velocity histogram in roughly the same velocity range, so this explanation may not be wholly correct.

Figure 10 shows how the KISS sample is dominated by intermediate- and low-luminosity galaxies, with a typical luminosity comparable to that of the Large Magellanic Cloud. A significant population of higher luminosity galaxies is also present, but the high-luminosity end of the distribution appears truncated when compared to the CGCG sample. This effect is due to the filter-induced redshift cut-off of the KISS sample, which causes the luminous end of the sample to become volume-limited. Hence, the KISS sample lacks the high luminosity tail that is commonly seen in magnitude-limited samples.

Even though there are large numbers of lower luminosity ELGs present in KISS, the proportion of dwarf star-forming systems is significantly lower than in [O III]-selected surveys like the UM survey and KB1. The median absolute magnitude for the UM ELGs is  $M_B = -18.1$  (Salzer *et al.* 1989), while that of KB1 is  $-18.0$ . Despite these differences in the median luminosities of the [O III]-selected vs. the  $H\alpha$ -selected samples, one should not conclude that the KISS sample is deficient in dwarf galaxies relative to the blue surveys. As demonstrated by the large overlap between the first blue survey list (KB1) and the first red survey list (KR1), the  $H\alpha$  survey technique is just as efficient at finding dwarf ELGs as is the [O III]-selection method. However,  $H\alpha$ -selected samples can detect many more higher-luminosity galaxies which tend to be missed by the [O III]-selected surveys. More luminous galaxies with starbursts tend to have weaker [O III] lines. In addition, [O III]-selected surveys tend to be biased against luminous galaxies due to the higher amounts of reddening present in these more metal-rich systems. Since KISS

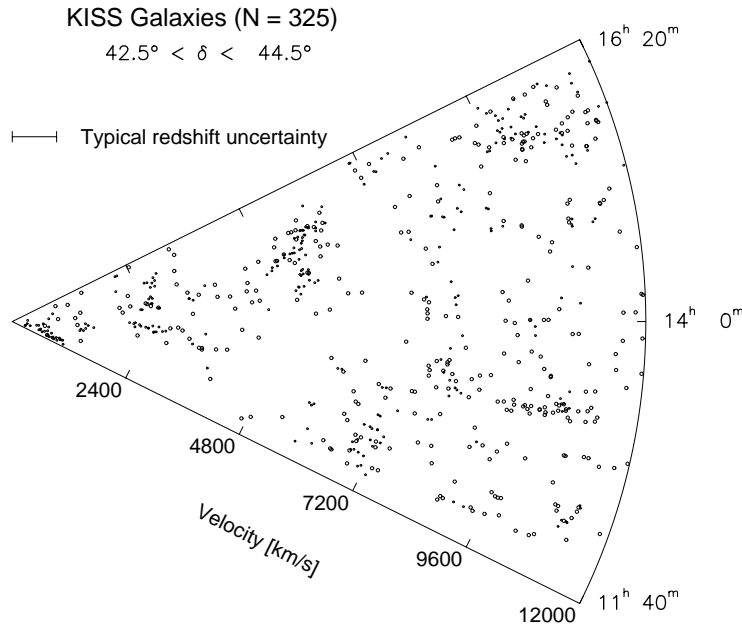


FIG. 11.— This plot compares the spatial distribution of ELGs to that of “normal” galaxies, out to velocities of  $12,000 \text{ km s}^{-1}$ . The “normal” galaxies are represented by CGCG galaxies from the declination range  $41^\circ < \delta < 46^\circ$ . Only 12 CGCG galaxies are found at velocities  $> 12,000 \text{ km s}^{-1}$ . The KISS galaxies are plotted as open circles, and the CGCG galaxies are overplotted as dots. At lower velocities the ELGs are seen to trace the large-scale structures defined by the CGCG galaxies. However, they appear to be less tightly clustered, and a large number of ELGs fall in voids.

selects by  $H\alpha$ , it does not suffer from these biases. The KISS sample should thus be a more representative catalog of AGN and star-forming galaxies.

#### 4.2.2. Spatial Distribution

Because of the depth and good redshift coverage of the KISS ELGs, it is also relevant to consider the spatial distribution of the sample. This is illustrated in Figures 11 and 12, which show cone diagrams for the KISS and CGCG galaxies. The redshifts plotted for the KISS galaxies are those from Table 2. The error bar shown in both figures illustrates the size of the formal uncertainty in our objective-prism redshifts ( $840 \text{ km s}^{-1}$ , see Section 4.1.3).

Figure 11 shows both the KISS and CGCG galaxies out to  $12,000 \text{ km s}^{-1}$  ( $z \leq 0.04$ ). At redshifts beyond about  $12,000 \text{ km s}^{-1}$ , the CGCG sample thins out drastically, and no longer can be used to delineate large-scale structure. The general impression obtained from examination of this figure is that the KISS ELGs tend to fall along the same large-scale structures as those traced out by the CGCG galaxies. However, the ELGs appear to be less tightly confined to the structures than are the “normal” galaxies. Because of the limited precision of the KISS redshifts ( $\pm 840 \text{ km s}^{-1}$ ), it is possible that the appearance of lower clustering is an artifact of the data (i.e., consider the size of the typical redshift error illustrated). However, the large numbers of galaxies located well into some of the voids present within this volume of space suggest that the lower level of clustering is in fact real. Previous studies of the spatial distribution of ELG samples have found similar

results (Salzer 1989, Rosenberg *et al.* 1994, Pustil’nik *et al.* 1995, Popescu *et al.* 1997, Lee *et al.* 2000). The lower level of clustering seen in Figure 11 is due primarily to lower-luminosity ELGs. We are currently analyzing the relative clustering strengths of the ELGs and CGCG galaxies, using more accurate redshifts from our follow-up spectra when available (Lee, Salzer & Gronwall 2004).

Figure 12 shows all KISS galaxies out to  $30,000 \text{ km s}^{-1}$  ( $z \leq 0.10$ ). The KISS galaxies are found in great numbers out to  $\sim 27,000 \text{ km s}^{-1}$ , beyond which the survey begins to be truncated by the filter. The approximate position of the Boötes void is indicated by the circle. We have chosen a rather conservative estimate for the radius of the void,  $r_{\text{void}} = 2,400 \text{ km s}^{-1}$  (most previous studies have adopted  $r_{\text{void}} = 3,000 \text{ km s}^{-1}$ ). It is clear from this figure that the depth of the KISS survey is sufficient to adequately sample the far side of the void. Based on our objective-prism redshifts, we find 12 objects that appear to be located inside the Boötes void (18 if we were to use  $r_{\text{void}} = 3,000 \text{ km s}^{-1}$ ), only one of which was known previously to be a void-dwelling object. The void galaxies have a median B magnitude of 18.25 (range 17.38 to 20.73) and a median absolute B magnitude of  $-18.56$  (range  $-16.02$  to  $-19.07$ ). Only one of the twelve galaxies has been observed spectroscopically by our group at this time. That object is KISSR 1943, which is a star-forming galaxy that happens to be the faintest and least luminous object of the twelve. The measured slit-spectrum redshift confirms its location within the void.

The ELGs in the cone diagram appear to indicate the

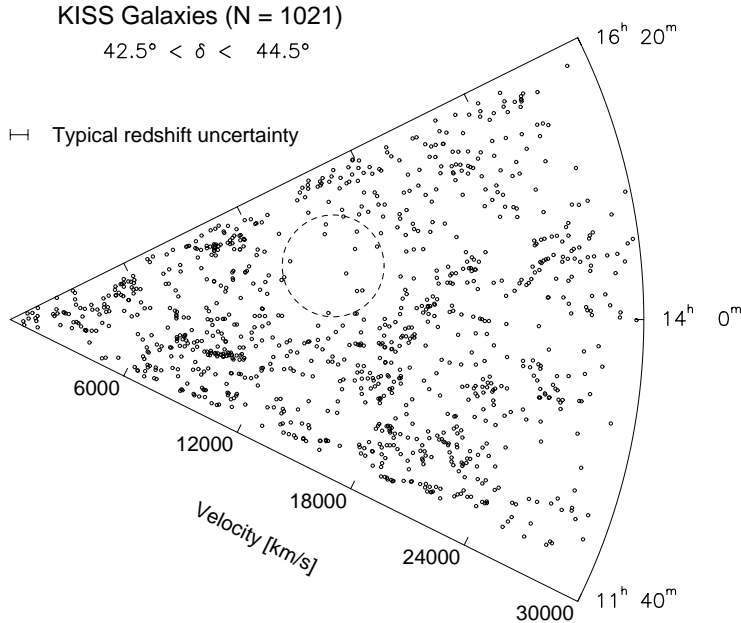


FIG. 12.— The spatial distribution of KISS galaxies is shown out to velocities of  $30,000 \text{ km s}^{-1}$ . The circle indicates the approximate position of the Boötes void. The numbers of ELGs remains high out to  $\sim 27,000 \text{ km s}^{-1}$ , the point where the survey filter cut-off begins to affect the sample. The KISS catalog is sufficiently deep to adequately sample the far side of the Boötes void. We also find 12 objects that appear to be located inside this void.

presence of a number of filaments and voids at these higher redshifts. The ELGs map out large-scale structures, albeit only roughly, out to  $z = 0.09$  without the need for follow-up spectra! While the limited velocity resolution, together with the tendency for the ELGs to be less clustered, prevents the use of these data for detailed definition of large-scale structures at these redshifts, they certainly provide a reasonable picture of the coarse outlines. Furthermore, since the KISS galaxies are selected due to their strong line emission, follow-up spectroscopy of these faint galaxies is relatively easy. Thus, using ELGs to trace out the main features in the spatial distribution of galaxies is an efficient use of telescope time.

#### 4.3. Comparison with Previous Surveys

Table 2 lists cross-references for KISS ELGs which are also cataloged in previous photographic surveys for active and star-forming galaxies. The first red KISS strip overlapped with four major surveys: Markarian (1967), Case (Pesch & Sanduleak 1983), Wasilewski (1983), and UCM (Zamorano *et al.* 1994). As described in KR1, all ELGs cataloged by the emission line-selected surveys (Wasilewski and UCM) were recovered by KISS. The second red survey strip, however, overlaps with only two surveys, both of which select sources based on their UV-excess (Markarian) or on a combination of UV-excess and emission lines (Case). We expect KISS to recover only a subset of the objects cataloged by these surveys; in the first red KISS strip, 73% of Markarian and Case objects were listed

either in the main survey or among the  $4\sigma$  to  $5\sigma$  objects. A similar fraction of objects from these catalogs was recovered in the second red survey strip, as detailed below.

There are 16 Markarian galaxies in the area of the second KISS survey strip; twelve of these (75%) were recovered by KISS in the main survey (i.e., Table 2). Of the four objects not found by KISS, one is beyond the redshift limit set by our survey filter and one has no redshift listed in the Markarian catalog. Inspection of the objective-prism spectra of the two remaining Markarian galaxies, Mrk 491 and Mrk 1475, revealed no evidence of line emission.

There are 55 Case objects in the KISS area. For one of them (CG 646) it is noted in the NASA/IPAC Extragalactic Database<sup>7</sup> that no object is present at the given position in the second Palomar Sky Survey images, and that this Case object may possibly have been a very faint dwarf nova. We therefore do not consider CG 646 to be a *bona fide* galaxy. Of the remaining 54 galaxies, 39 were recovered by KISS in the main survey (72%). We examined the 15 Case galaxies not recovered by KISS, and found that eight are listed in the Case Survey papers as being color-selected, and four are listed as having questionable (w? or w:) line detections. Only three of the unrecovered galaxies are listed as having strong or medium-strength emission lines. Careful examination of the KISS objective-prism spectra for these objects shows that one galaxy (CG 501) appears to have emission lines, but they are too weak for it to be included in the KISS catalog. The objective-

<sup>7</sup> The NASA/IPAC Extragalactic Database (NED) is operated by the Jet Propulsion Laboratory, California Institute of Technology, under contract with the National Aeronautics and Space Administration.

prism spectra of the other two galaxies (CG 536 and CG 902) show no evidence of line emission. Spectroscopy of 61 Case galaxies by Salzer *et al.* (1995) in the red portion of the spectrum found that 31% had H $\alpha$  equivalent widths less than 30 Å. Hence, it would appear that the majority of non-detected Case galaxies belong to the weak-lined subsample of the Case survey, to which KISS is not sensitive.

## 5. SUMMARY

We present the second list of H $\alpha$ -selected emission-line galaxy candidates (and third list overall) from the KPNO International Spectroscopic Survey (KISS). All data presented here were obtained with the 0.61-m Burrell Schmidt telescope. KISS is an objective-prism survey, but differs from older such surveys by virtue of the fact that it utilizes a CCD as the detector. While we sacrifice areal coverage relative to classical photographic surveys, we benefit from the enormous gain in sensitivity that CCDs provide over plates. We readily detect strong-lined ELGs as faint as  $B = 21$ . In addition, the pan-chromatic nature of CCDs allows us greater wavelength agility compared to photographic surveys. In combination with our survey filter we are sensitive to a broader range of galaxian redshifts than the older photographic objective-prism surveys (Paper I). The combination of higher sensitivity, lower noise, and larger volumes surveyed yield huge improvements in the depth of the resulting survey. KISS finds 169 times more AGN and starburst galaxy candidates per unit area than did the Markarian (1967) survey, and 30 times more than the UCM survey (Zamorano *et al.* 1994).

The current installment of KISS includes 1029 ELG candidates selected from 62 red survey fields covering a total of 65.8 deg<sup>2</sup>. This yields a surface density of 15.6 galaxies per deg<sup>2</sup>. The two red survey lists combined (KR1 plus the current) cover an area of 128 square degrees with a surface density of nearly 17 galaxies per deg<sup>2</sup>. We are sensitive to the H $\alpha$  emission line with redshifts up to  $\sim 0.10$ . Our survey follows a narrow strip across the sky at a declination of  $\delta(1950) = 43^\circ 30'$  and spans the RA range  $11^h 55^m$  to  $16^h 15^m$ . This region was chosen to pass through the center of the Boötes void (Kirshner *et al.* 1981). For each object in the catalog we tabulate accurate equatorial coordinates, B & V photometry, and estimates of the redshift and line strength measured from the objective-prism spectra. Also provided are finder charts and extracted spectral plots for all galaxies. In addition to the main survey list, we include a supplementary list of 291 ELG candidates with weaker (lower significance) emission lines.

One of the advantages of our survey method is the large amount of basic data that we acquire for each object. This in turn allows us to parameterize the constituents of the survey and to develop a fairly complete picture of the overall sample without the need for extensive follow-up observations. We present an overview of the survey properties for the current list of ELG candidates. The median apparent magnitude of the sample is  $B = 18.13$ , which agrees

well with the value found for KR1 ( $B = 18.08$ ), and which is substantially fainter than previous ELG surveys. Objects fainter than  $B = 20$  are routinely cataloged. Line strengths measured from the objective-prism spectra show that KISS is sensitive to objects with H $\alpha$  + [N II] equivalent widths of less than 20 Å, and that most objects with  $EW > 30$  Å are detected. The median emission-line flux of the KISS sample is more than three times lower than that of the UCM survey (Gallego *et al.* 1996). The luminosity distribution of the KISS ELGs is heavily weighted toward intermediate- and low-luminosity galaxies, although we are still sensitive to luminous AGN and starbursting galaxies. The median absolute magnitude of  $M_B = -18.67$  underscores the fact that strong-lined galaxies of the type cataloged by KISS tend to be less luminous than the types of objects found in more traditional magnitude-limited samples.

While we stressed above that one can learn a great deal about each KISS ELG from the survey data alone, it is still necessary to obtain higher dispersion follow-up spectra in order to arrive at a more complete understanding of each object. For example, the low-dispersion nature of the objective-prism spectra does not allow us to distinguish between AGN and star-formation activity in the KISS galaxies. Further, the redshifts derived from the KISS spectral data are too coarse to be used in detailed spatial distribution studies (e.g., Lee, Salzer & Gronwall 2004). We are in the process of obtaining spectra for a large number of KISS ELGs from all three survey lists (KR1, KB1, and the current list) in order to better assess the nature of the individual galaxies. This in turn enables the sample to be used for a wide variety of science applications, many of which are outlined in Paper I. Examples include a series of multi-wavelength studies of the properties of KISS ELGs in the radio (Van Duyne *et al.* 2004) and X-rays (Stevenson *et al.* 2002), plus studies currently underway in the far-IR (IRAS) and near-IR (2MASS).

We gratefully acknowledge financial support for the KISS project through NSF Presidential Faculty Award to JJS (NSF-AST-9553020), which was instrumental in allowing for the international collaboration, as well as continued support via NSF-AST-0071114. CG also acknowledges support from NSF-AST-0137927. Several useful suggestions by the anonymous referee helped to improve the presentation of this paper. We thank the numerous colleagues with whom we have discussed the KISS project over the past several years, including Jesús Gallego, Rafael Guzmán, Rob Kennicutt, David Koo, Trinh Thuan, Alexei Kniazev, Yuri Izotov, Janice Lee, Jason Melbourne and Jose Herrero. Finally, we wish to thank Heather Morrison, Paul Harding, and the Astronomy Department of Case Western Reserve University for maintaining the Burrell Schmidt during the period of time when the survey observations reported here were obtained.

## APPENDIX

### SUPPLEMENTARY TABLE OF $4\sigma$ OBJECTS

As discussed in Section 3, our selection method has produced a list of objects with apparent emission lines with strengths that are slightly weaker than the  $5\sigma$  limit imposed on the main survey objects. Because one of the primary goals of the

KISS project is to construct a deep but statistically complete sample of ELGs, we made the decision to exclude these objects from the main survey list. However, these objects are nonetheless valid ELG candidates, and this list of sources likely includes a number of interesting objects. Therefore, rather than ignore these weaker-lined ELG candidates entirely, we are publishing them in a supplementary table.

Listed in Table 4 are 291 ELG candidates that have emission lines detected at between the  $4\sigma$  and  $5\sigma$  level. The format of Table 4 is the same as for Table 2, except that the objects are now labeled with KISSRx numbers ('x' for extra). The KISSRx numbers start at 190 since we presented 189 KISSRx objects in KR1. The full version of the table, as well as finder charts for all 291 KISSRx galaxies, are available in the electronic version of the paper.

The characteristics of the supplementary ELG sample are similar to those of the main survey ELGs, although with some notable differences. The median  $H\alpha$  equivalent width is 29.5 Å, roughly a third lower than the value for the main sample. The KISSRx galaxies are somewhat fainter (median B magnitude of 18.77) and significantly redder (median  $B-V = 0.77$ ). Their median redshift is slightly higher than that of the main sample (0.068), and their median luminosity is slightly lower ( $-18.27$ ). Hence, the supplementary ELG list appears to be dominated by intermediate luminosity galaxies with a significantly lower rate of star-formation activity (lower equivalent widths, redder colors) than the ELGs in the main sample. The differences between the KISSR and KISSRx objects in the current paper are similar to those seen between the two samples in KR1.

## REFERENCES

- Aldering, G. S. 1990, PhD Thesis, University of Michigan
- Falco, E. E., Kurtz, M. J., Geller, M. J., Huchra, J. P., Peters, J., Berlind, P., Mink, D. J., Tokarz, S. P., & Elwell, B. 1999, *PASP*, 111, 438
- Fukugita, M., Shimasaku, K., & Ichikawa, T. 1995, *PASP*, 107, 945
- Gallego, J., Zamorano, J., Rego, M., Alonso, O., & Vitores, A. G. 1996, *A&AS*, 120, 323
- Gronwall, C., Salzer, J. J., Brenneman, L., Condy, E., & Santos, M. 2004, in preparation
- Huchra, J. P., & Sargent, W. L. W. 1973, *ApJ*, 186, 433
- Kirshner, R. P., Oemler, A., Jr., Schechter, P. L., & Shectman, S. A. 1981, *ApJ*, 248, L57
- Kirshner, R. P., Oemler, A., Jr., Schechter, P. L., & Shectman, S. A. 1983, in *IAU Symposium 104, Early Evolution of the Universe and Its Present Structure*, eds. G. O. Abell and G. Chincarini (Dordrecht: Reidel), p. 97
- Kirshner, R. P., Oemler, A., Jr., Schechter, P. L., & Shectman, S. A. 1987, *ApJ*, 314, 493
- Lee, J. C., Salzer, J. J., & Gronwall, C. 2004, in preparation
- Lee, J. C., Salzer, J. J., Law, D. A., & Rosenberg, J. L. 2000, *ApJ*, 536, 606
- MacAlpine, G. M., Smith, S. B., & Lewis, D. W. 1977, *ApJS*, 34, 95
- Markarian, B. E. 1967, *Astrofizika*, 3, 55
- Markarian, B. E., Lipovetskii, V. A., & Stepanian, D. A. 1983, *Astrofizika*, 19, 29
- Mazzarella, J. M., & Balzano, V. A. 1986, *ApJS*, 62, 751
- Moody, J. W., Kirshner, R. P., MacAlpine, G. M., & Gregory, S. A. 1987, *ApJ*, 314, 33
- Nilson, P. 1973, *Uppsala General Catalogue of Galaxies*, (Uppsala: Roy. Soc. Sci. Uppsala)
- Pérez-González, P. G., Zamorano, J., Gallego, J., & Gil de Pez, A. 2000, *A&AS*, 141, 409
- Pesch, P., & Sanduleak, N. 1983, *ApJS*, 51, 171
- Popescu, C. C., Hopp, U., & Elsässer, H. 1997, *A&A*, 328, 756
- Popescu, C. C., Hopp, U., Hagen, H. J., & Elsässer, H. 1996, *A&AS*, 116, 43
- Pustil'nik, S., Ugryumov, A. V., Lipovetsky, V. A., Thuan, T. X., & Guseva, N. 1995, *ApJ*, 443, 499
- Roberts, M. S., & Haynes, M. P. 1994, *ARA&A*, 32, 115
- Rosenberg, J. L., Salzer, J. J., & Moody, J. W. 1994, *AJ*, 108, 1557
- Salzer, J. J. 1989, *ApJ*, 347, 152
- Salzer, J. J., Gronwall, C., Lipovetsky, V. A., Kniazev, A., Moody, J. W., Boroson, T. A., Thuan, T. X., Izotov, Y. I., Herrero, J. L., & Frattare, L. M. 2000, *AJ*, 120, 80 (Paper I)
- Salzer, J. J., Gronwall, C., Lipovetsky, V. A., Kniazev, A., Moody, J. W., Boroson, T. A., Thuan, T. X., Izotov, Y. I., Herrero, J. L., & Frattare, L. M. 2001, *AJ*, 121, 66 (KR1)
- Salzer, J. J., Gronwall, C., Sarajedini, V. L., Lipovetsky, V. A., Kniazev, A., Moody, J. W., Boroson, T. A., Thuan, T. X., Izotov, Y. I., Herrero, J. L., & Frattare, L. M. 2002, *AJ*, 123, 1292 (KB1)
- Salzer, J. J., MacAlpine, G. M., & Boroson, T. A. 1989, *ApJS*, 70, 479
- Salzer, J. J., Moody, J. W., Rosenberg, J. L., Gregory, S. A., & Newberry, M. V. 1995, *AJ*, 109, 2376
- Sanduleak, N. & Pesch, P. 1982, *ApJ*, 258, 11
- Sanduleak, N. & Pesch, P. 1987, *ApJS*, 63, 809
- Schechter, P. L. 1976, *ApJ*, 203, 297
- Schlegel, D. J., Finkbeiner, D. P., & Davis, M. 1998, *ApJ*, 500, 525
- Schmidt, M. 1968, *ApJ*, 151, 393
- Smith, M. G., Aguirre, C., & Zelman, M. 1976, *ApJS*, 32, 217
- Stevenson, S. L., Salzer, J. J., Sarajedini, V. L., & Moran, E. C. 2002, *AJ*, 124, 3465
- Surace, C., & Comte, G. 1998, *A&AS*, 133, 171
- Ugryumov, A. V., *et al.* 1999, *A&AS*, 135, 511
- Van Duyne, J., Beckerman, E., Salzer, J. J., Gronwall, C., Thuan, T. X., Condon, J. J., & Frattare, L. M. 2004, *AJ*, submitted
- Wasilewski, A. J. 1983, *ApJ*, 272, 68
- Wegner, G., Salzer, J. J., Jangren, A., Gronwall, C., & Melbourne, J. 2003, *AJ*, 125, 2373
- Zamorano, J., Rego, M., Gallego, J., Vitores, A.G., González-Riestra, R., & Rodríguez-Caderot, G. 1994, *ApJS*, 95, 387
- Zwicky, F., Herzog, E., Kowal, C. T., Wild, P., & Karpowicz, M. 1961–1968, *Catalogue of Galaxies and Clusters of Galaxies*, (Pasadena: CIT) (CGCG)



TABLE 1  
KISS 43° RED SURVEY OBSERVING RUNS

Dates of Run (1)	Number of Nights <sup>a</sup> (2)	Number of Fields – Direct <sup>b</sup> (3)	Number of Fields – Spectral <sup>b</sup> (4)
April 19 – May 4, 1998	15	43	40
June 19 – 21, 1998	3	7	...
May 7 – 14, 1999	8	12	22

<sup>a</sup>Number of nights during run that data were obtained.

<sup>b</sup>Number of survey fields observed.

TABLE 2  
LIST OF CANDIDATE ELGS

KISSR # (1)	Field (2)	ID (3)	R.A. (J2000) (4)	Dec. (J2000) (5)	B (6)	B-V (7)	$z_{KISS}$ (8)	Flux <sup>a</sup> (9)	EW [Å] (10)	Qual. (11)	Comments (12)
1129	F1155	5259	11 53 51.3	42 48 00.7	20.84	1.08	-0.0076	66	84	2	
1130	F1155	5256	11 54 08.8	43 23 22.5	18.52	0.50	0.0440	56	71	1	
1131	F1155	5038	11 54 10.5	43 06 01.5	18.13	0.77	0.0668	91	31	1	
1132	F1155	5324	11 54 10.5	43 32 54.2	17.58	0.56	0.0662	161	67	1	
1133	F1155	5234	11 54 15.1	43 34 00.9	16.77	0.75	0.0666	485	63	1	
1134	F1155	5003	11 54 15.7	43 13 36.1	16.46	0.57	0.0157	126	12	1	CG 1472
1135	F1155	4840	11 54 18.7	43 06 57.4	18.26	0.46	0.0656	68	64	2	
1136	F1155	4700	11 54 23.9	43 05 09.8	15.94	0.77	0.0677	530	48	1	
1137	F1155	4797	11 54 25.1	43 16 59.2	17.17	0.69	0.0543	237	47	1	
1138	F1155	4513	11 54 29.4	42 58 48.5	16.30	0.87	0.0231	217	14	1	
1139	F1155	4526	11 54 33.7	43 08 12.8	18.67	0.50	0.0867	107	97	1	
1140	F1155	4556	11 54 35.6	43 14 57.9	16.34	0.96	0.0674	252	21	1	
1141	F1155	4280	11 54 45.0	43 09 54.0	16.87	0.92	0.0678	240	31	1	
1142	F1155	3983	11 54 58.6	43 11 38.5	19.39	0.77	0.0898	41	63	2	
1143	F1155	3513	11 55 32.0	43 31 29.1	17.80	0.47	0.0349	251	118	1	
1144	F1155	2966	11 55 35.4	42 46 35.5	19.56	0.50	0.0836	66	292	2	
1145	F1155	3534	11 55 35.8	43 40 34.7	19.36	0.54	0.0499	71	253	1	
1146	F1155	3081	11 55 38.4	43 02 44.2	14.59	0.78	0.0294	788	20	1	UGC 6901, CG 1477
1147	F1155	3518	11 55 40.6	43 48 39.7	17.08	1.09	0.0904	55	7	1	CG 1478
1148	F1155	3479	11 55 43.5	43 50 41.9	17.91	0.57	0.0728	255	130	1	
1149	F1155	3531	11 55 50.4	44 08 06.6	16.45	0.94	0.0734	253	31	1	
1150	F1155	3044	11 55 57.1	43 35 34.2	15.30	0.51	0.0358	333	17	1	Mk 1464, CG 1480
1151	F1155	3301	11 55 57.6	43 59 09.0	19.22	0.77	0.0733	33	35	3	
1152	F1155	2836	11 56 12.0	43 45 10.1	19.06	0.44	0.0486	72	122	1	
1153	F1155	2596	11 56 24.7	43 48 01.8	18.27	0.61	0.0694	129	113	1	
1154	F1155	1892	11 56 32.9	42 59 38.8	16.30	0.76	0.0747	324	46	1	
1155	F1155	1803	11 57 04.5	43 49 37.0	16.34	0.84	0.0247	344	25	1	
1156	F1155	1159	11 57 15.1	43 15 58.4	18.72	0.69	0.0901	39	34	1	
1157	F1155	1538	11 57 17.5	43 49 47.7	17.50	0.49	0.0251	189	67	1	
1158	F1155	1282	11 57 32.1	43 57 16.1	17.33	0.73	0.0704	272	59	1	

Note. – The complete version of this table is presented in the electronic edition of the Journal. A portion is shown here for guidance regarding its content and format.

<sup>a</sup>Units of  $10^{-16}$  erg/s/cm<sup>2</sup>

TABLE 3  
 $V/V_{max}$  TEST

$m_L$	Total Number	Number Flux Limited	Number Volume Limited	$\langle V/V_{max} \rangle$	Number added	Cumulative number added	% Flux Limited	% Complete
(1)	(2)	(3)	(4)	(5)	(6)	(7)	(8)	(9)
13.0	17	17	0	0.5485	0	0	100.00	100.00
13.1	21	20	1	0.5794	0	0	95.24	100.00
13.2	26	25	1	0.5906	0	0	96.15	100.00
13.3	30	28	2	0.5687	0	0	93.33	100.00
13.4	34	32	2	0.5520	0	0	94.12	100.00
13.5	42	39	3	0.5656	0	0	92.86	100.00
13.6	47	42	5	0.5499	0	0	89.36	100.00
13.7	55	46	9	0.5382	0	0	83.64	100.00
13.8	71	58	13	0.5843	0	0	81.69	100.00
13.9	75	60	15	0.5258	0	0	80.00	100.00
14.0	87	65	22	0.5582	0	0	74.71	100.00
14.1	105	79	26	0.5777	0	0	75.24	100.00
14.2	128	102	26	0.5993	0	0	79.69	100.00
14.3	150	116	34	0.5932	0	0	77.33	100.00
14.4	177	138	39	0.5889	0	0	77.97	100.00
14.5	209	157	52	0.5903	0	0	75.12	100.00
14.6	238	175	63	0.5768	0	0	73.53	100.00
14.7	277	193	84	0.5757	0	0	69.68	100.00
14.8	308	213	95	0.5528	0	0	69.16	100.00
14.9	346	236	110	0.5444	0	0	68.21	100.00
15.0	393	256	137	0.5480	0	0	65.14	100.00
15.1	431	262	169	0.5267	0	0	60.79	100.00
15.2	476	276	200	0.5192	0	0	57.98	100.00
15.3	520	302	218	0.5108	0	0	58.08	100.00
15.4	579	323	256	0.5122	0	0	55.79	100.00
15.5	630	340	290	0.5039	0	0	53.97	100.00
15.6	683	364	319	0.4983	1	1	53.29	99.73
15.7	728	371	357	0.4824	12	13	50.96	96.61
15.8	773	388	385	0.4745	10	23	50.19	94.40
15.9	815	403	412	0.4577	20	43	49.45	90.36
16.0	859	405	454	0.4423	23	66	47.15	85.99
16.1	901	416	485	0.4264	29	95	46.17	81.41
16.2	923	388	535	0.3900	44	139	42.04	73.62
16.3	955	380	575	0.3719	41	180	39.79	67.86
16.4	977	359	618	0.3571	41	221	36.75	61.90
16.5	998	345	653	0.3373	51	272	34.57	55.92
16.6	1008	332	676	0.3106	64	336	32.94	49.70
16.7	1014	317	697	0.2769	75	411	31.26	43.54
16.8	1016	296	720	0.2416	83	494	29.13	37.47
16.9	1018	268	750	0.2164	82	576	26.33	31.75
17.0	1019	244	775	0.1941	91	667	23.95	26.78

TABLE 4  
LIST OF  $4\sigma$  CANDIDATE ELGS

KISSRx # (1)	Field (2)	ID (3)	R.A. (J2000) (4)	Dec. (J2000) (5)	B (6)	B-V (7)	$z_{KISS}$ (8)	Flux <sup>a</sup> (9)	EW [Å] (10)	Qual. (11)	Comments (12)
190	F1155	5353	11 54 10.0	43 33 31.1	18.45	0.46	0.0671	27	28	3	
191	F1155	4820	11 54 23.2	43 14 35.6	18.33	0.81	0.0879	39	17	3	
192	F1155	4935	11 54 30.9	43 38 55.9	17.78	0.98	0.0890	21	5	3	
193	F1155	3506	11 55 35.7	43 38 07.4	18.67	0.74	0.0746	106	115	2	
194	F1155	3327	11 55 54.9	43 56 32.8	16.08	0.54	0.0246	165	21	2	
195	F1155	2903	11 56 14.0	43 55 18.8	18.64	0.53	0.0774	39	48	3	
196	F1155	1846	11 57 00.9	43 47 43.7	19.13	0.63	0.0480	52	67	3	
197	F1155	256	11 57 37.7	42 43 19.9	18.00	0.84	0.0738	59	24	2	
198	F1200	5996	11 58 28.5	43 04 31.7	16.68	0.62	0.0173	36	5	3	
199	F1200	2782	12 00 09.8	44 08 40.0	18.86	0.63	0.0836	56	89	3	
200	F1200	1587	12 00 58.5	44 09 05.4	18.04	0.69	0.0035	52	20	2	
201	F1200	1639	12 01 15.4	43 19 09.3	19.62	0.85	0.0809	23	73	3	
202	F1200	1157	12 01 36.1	43 17 23.6	18.67	1.05	0.0692	45	19	2	
203	F1204	6213	12 02 53.5	42 52 35.4	20.06	1.03	0.0927	56	81	2	
204	F1204	5164	12 02 59.6	44 04 07.1	21.30	2.01	0.0726	31	41	2	
205	F1204	4187	12 03 48.8	43 28 28.6	17.94	0.81	0.0761	80	42	2	
206	F1204	2054	12 05 31.4	42 39 01.2	19.34	0.69	0.0544	41	66	2	
207	F1208	4425	12 07 53.7	43 20 50.0	18.62	0.90	0.0667	56	35	2	
208	F1208	3147	12 08 52.8	42 51 34.7	20.44	1.65	0.0728	55	34	2	
209	F1212	2565	12 13 16.8	44 09 25.4	20.39	1.86	0.0831	21	24	3	
210	F1212	2767	12 13 27.7	43 22 50.7	20.77	0.71	0.0682	46	430	3	
211	F1212	1358	12 14 02.2	43 52 17.1	19.30	1.10	0.0681	35	33	3	
212	F1212	794	12 14 22.3	43 53 45.5	19.15	0.51	0.0922	47	76	3	
213	F1212	146	12 15 07.0	42 54 47.7	18.46	0.94	0.0600	42	23	3	
214	F1217	4382	12 16 42.9	43 40 41.8	17.76	0.59	0.0412	38	13	2	
215	F1217	3456	12 17 36.7	42 48 30.6	18.43	0.62	0.0868	48	48	2	
216	F1217	1873	12 18 08.2	43 53 24.6	18.97	0.83	0.0659	19	19	3	
217	F1217	1750	12 18 23.5	43 24 55.9	18.16	0.48	0.0449	26	18	2	
218	F1221	6045	12 19 42.2	43 52 10.5	16.92	0.53	0.0499	46	14	2	
219	F1221	3278	12 21 26.7	43 52 56.0	17.62	0.75	0.0454	82	25	1	

Note.— The complete version of this table is presented in the electronic edition of the Journal. A portion is shown here for guidance regarding its content and format.

<sup>a</sup>Units of  $10^{-16}$  erg/s/cm<sup>2</sup>